Title
Rab7—a novel redox target that modulates inflammatory pain processing

Journal
Pain, 158(7)

ISSN
0304-3959

Authors
Kallenborn-Gerhardt, Wiebke
Möser, Christine V
Lorenz, Jana E
et al.

Publication Date
2017-07-01

DOI
10.1097/j.pain.0000000000000920

Research Paper

PAIN®

Rab7—a novel redox target that modulates inflammatory pain processing

Wiebke Kallenborn-Gerhardt[a,b,*], Christine V. Möser[b], Jana E. Lorenz[b], Mirco Steger[c], Juliana Heidler[c], Reynir Scheving[b], Jonas Petersen[a,d], Lea Kennel[a], Cathrin Flauaus[a], Ruirui Lu[a,d], Aimee L. Edinger[f], Irmgard Tegeder[b], Gerd Geisslinger[b,e], Heinrich Heide[c], Ilka Wittig[c], Achim Schmidtko[a,d]

Abstract

Chronic pain is accompanied by production of reactive oxygen species (ROS) in various cells that are important for nociceptive processing. Recent data indicate that ROS can trigger specific redox-dependent signaling processes, but the molecular targets of ROS signaling in the nociceptive system remain largely elusive. Here, we performed a proteome screen for pain-dependent redox regulation using an OxICAT approach, thereby identifying the small GTPase Rab7 as a redox-modified target during inflammatory pain in mice. Prevention of Rab7 oxidation by replacement of the redox-sensing thiols modulates its GTPase activity. Immunofluorescence studies revealed Rab7 expression to be enriched in central terminals of sensory neurons. Knockout mice lacking Rab7 in sensory neurons showed normal responses to noxious thermal and mechanical stimuli; however, their pain behavior during inflammatory pain and in response to ROS donors was reduced. The data suggest that redox-dependent changes in Rab7 activity modulate inflammatory pain sensitivity.

Keywords: Rab7, Redox proteomics, Reactive oxygen species, Inflammatory pain, Knockout mice

1. Introduction

Chronic pain is characterized by sensitization of the nociceptive system leading to increased responses to noxious stimuli (hyperalgesia), increased responses to normally innocuous stimuli (allodynia), and to spontaneous pain in the absence of any stimulus. As currently available treatments are only partially effective and associated with severe side effects, it is important to elucidate molecular mechanisms of nociceptive processing to develop novel strategies for chronic pain treatment.[1,30,31] Emerging lines of evidence suggest that reactive oxygen species (ROS) such as superoxide (O_2^-) or hydrogen peroxide (H_2O_2) are generated in nociceptive pathways and contribute to pain sensitization in a specific manner.[36,65] A specific function of ROS in chronic pain processing is supported at the behavioral level by data from mice lacking the ROS-producing NADPH oxidases Nox1, Nox2, or Nox4. These mice showed reduced hypersensitivity in models of inflammatory or neuropathic pain.[26,27,32,35,38,43] Moreover, administration of ROS scavengers and antioxidants reduced the pain behavior in various animal models,[39,47,62,70] whereas deficiency of antioxidant proteins enhanced the pain behavior.[2,34,69]

Specific redox signaling most often involves reversible oxidation of thiol residues within proteins thus changing structural and functional characteristics that may alter protein function.[37,64] In general, several proteins, including transient receptor potential (TRP) ion channels, N-methyl-D-aspartate (NMDA) receptors, T-type calcium channels, and $GABA_A$ receptors, have been found to sense ROS and change their activity in a redox-dependent manner.[13,40] However, to date only few specific redox targets of ROS-dependent pain processing have been identified. Recent redox-proteome approaches make use of altered biotin switch techniques in combination with liquid chromatography–mass spectrometry (LC-MS)/mass spectrometry (MS) analysis which allows for screening of redox-modified proteins within tissues. To identify redox-regulated proteins in the nociceptive synapse of the spinal cord of mice, we took advantage of the OxICAT method.[42] With this technique, reduced and oxidized thiols are differentially labeled using isotope-coded affinity tags (ICATs), which are subsequently detected and quantified by LC-MS/MS analysis.

One of the redox-regulated proteins we identified in our screen was the small Guanosine-5′-triphosphate (GTP)ase Rab7 that plays a key role in late-endosomal trafficking, promoting fusion of endosomes, phagosomes, and autophagosomes with the lysosome.[75,76] Rab7 activation is mediated by various regulators, including guanine-nucleotide exchange factors and other regulators such as homotypic fusion and protein sorting complexes, RILP (Rab7-interacting lysosomal protein) or FYCO1 (Fab1-YotB-Vac1p-EEA1 and coiled-coil domain containing 1) that facilitate Rab7 prenylation and membrane recruitment.[25,75] Of interest, Rab7 shows a high homology between species and mutations of

Sponsorships or competing interests that may be relevant to content are disclosed at the end of this article.

[a] *Institute of Pharmacology, College of Pharmacy, Goethe University, Frankfurt am Main, Germany,* [b] *Pharmazentrum Frankfurt/ZAFES, Institute of Clinical Pharmacology, Goethe University, Frankfurt am Main, Germany,* [c] *Functional Proteomics, SFB815 Core Unit, Goethe University, Frankfurt am Main, Germany,* [d] *Institute of Pharmacology and Toxicology, ZBAF, Witten/Herdecke University, Witten, Germany,* [e] *Fraunhofer Institute for Molecular Biology and Applied Ecology—Project Group Translational Medicine and Pharmacology (IME-TMP), Frankfurt am Main, Germany,* [f] *Developmental and Cell Biology, University of California, Irvine, CA, USA*

**Corresponding author. Address: Institute of Pharmacology, College of Pharmacy, Goethe University, Biozentrum N260, Max-von Laue Straße 9, D-60438 Frankfurt am Main, Germany. Tel.: +49 69 798 29365; fax: +49 69 798 29374. E-mail address: kallenborn@med.uni-frankfurt.de (W. Kallenborn-Gerhardt).*

PAIN 158 (2017) 1354–1365

http://dx.doi.org/10.1097/j.pain.0000000000000920

Rab7 or its interaction partners have been linked to various physiological disorders. For example, Rab7 mutations have been connected to Charcot–Marie–Tooth disease 2B (CMT2B), and defects of Rab5- and Rab7-mediated endosomal trafficking are related to Alzheimer disease, Down syndrome, and Parkinson disease.[5,8,10,12,24,56,73,74,76,77] In this study, we characterized the expression of Rab7 in the nociceptive system and its putative pain-relevant functions. Our data suggest that Rab7 is a specific redox target that modulates inflammatory pain processing.

2. Materials and methods

2.1. Animals

Tissue expression studies were performed in male C57BL/6N mice (Harlan). In addition, Rab7-deficient mice of either sex on a C57BL/6 background were used for behavioral studies. Generation of "floxed" Rab7 mice ($Rab7^{fl/fl}$) has been described previously.[63] To obtain conditional knockout mice lacking Rab7 in primary afferent neurons, $Rab7^{fl/fl}$ mice were crossed with mice expressing the Cre recombinase under control of the Advillin promoter.[21] Resulting heterozygous and homozygous conditional Rab7 knockouts are referred to as Adv-$Rab^{-/-}$ and Adv-$Rab7^{+/-}$, respectively. Animals were housed on a 12/12 hours light/dark cycle with free access to water and food. All experiments were approved by the local Ethics Committee for Animal Research and adhered to the guidelines of the Committee for Research and Ethical Issues of the International Association for the Study of Pain.

2.2. Redox proteomics

2.2.1. Sample preparation

To quantitatively identify redox-modified cysteines in the spinal cord, the OxICAT protocol by Leichert et al.[42] was used with some adaptation to mouse tissue. The cleavable ICAT method development and cleavable ICAT reagent kits were obtained from AB SCIEX (Darmstadt, Germany). Fifteen microliters of a zymosan A suspension (5 mg/mL in 0.1 M phosphate-buffered saline [PBS], pH 7.4; Sigma-Aldrich, Schnelldorf, Germany) was injected into the plantar subcutaneous space of a mouse hind paw.[52] Eight hours thereafter, lumbar spinal cords (L4-L5) of zymosan-injected and naive control animals were dissected out and immediately snap frozen in liquid nitrogen. Samples were weighed, homogenized in ice-cold 10% trichloroacetic acid (TCA), and a volume corresponding to 0.5 mg total tissue was used for further analysis. Samples were centrifuged for 30 minutes (13,000*g*, 4°C), and TCA precipitates were consecutively washed in 10% and 5% ice-cold TCA. Resulting pellets were dissolved in denaturing alkylation buffer (8 M urea, 10 mM EDTA, 200 mM TrisHCl, pH 8.5) containing 0.5% sodium dodecyl sulfate (SDS). The contents of one light ICAT reagent vials were dissolved in 10 μL acetonitrile, and 5 μL were transferred to each sample. Samples were incubated for 75 minutes at 37°C and 1300 rpm in the dark. Light ICAT reagent was removed by precipitation of proteins with ice-cold acetone over night at −20°C. The samples were then washed twice with ice-cold acetone, dissolved in 50 μL denaturing alkylation buffer buffer, and reduced with 1 μL of reducing reagent (50 mM Tris(2-carboyethyl)phosphine [TCEP]) provided in the kit for 5 minutes at 37°C and 1300 rpm. Heavy ICAT reagent was dissolved in acetonitrile and added to samples, which were incubated for 2 hours at 37°C and 1300 rpm in the dark. Samples were digested with trypsin for 16 hours at 37°C. Peptides were acidified by adding 20 μL pure formic acid and purified with solid phase extraction cartridges (Empore 4115(SD); Sigma Aldrich, St. Paul, MA). Enrichment of ICAT-labeled peptides on avidin columns and cleavage of biotin moiety from the isotope coded tag were performed as described in the manufacturers' manual.

2.2.2. LC-MS/MS analysis

LC/MS was performed on a Thermo Scientific Orbitrap XL mass spectrometer linked to an Agilent1200 nano–high-performance liquid chromatography. Peptides were resolved in 4% acetonitrile and 0.5% formic acid and loaded on a C18 reversed-phase precolumn (Zorbax 300SB-C18; Agilent Technologies, Palo Alto, CA) followed by separation on an in-house packed 3 μm Reprosil C18 resin (Dr. Maisch GmbH, Ammerbuch, Germany) picotip emitter tip (diameter 75 μm, length 10 cm; New Objectives, Woburn, MA) using a gradient from 5% acetonitrile, 0.1% formic acid to 50% acetonitrile, 0.1% formic acid for 90 minutes with a flow rate of 200 nL/min. MS data were recorded by data-dependent Top10 acquisition selecting the 10 most abundant precursor ions in positive mode for fragmentation using dynamic exclusion of 3 minutes. Only highly charged ions (2+) were selected for MS/MS scans in the linear ion trap by CID at 35% collision energy. Lock mass option for m/z 445.120,025 was enabled to ensure high mass accuracy during many following runs.[57]

2.2.3. Data analysis

MS data were searched using Mascot Server (version 2.2) against a database containing species-specific (*Mus musculus*) protein sequences downloaded from www.uniprot.org. The Mascot search settings were as follows: maximum missed cleavages 1, precursor mass tolerance 10 ppm, fragment ion tolerance 0.8 Da, and optional modifications allowed on methionine (oxidation) and cysteine. Only peptides with individual ion scores indicating identity ($P < 0.05$) were considered significant. Quantification of heavy/light ICAT ratios of peptides was performed by Proteome Discoverer 1.2. Peptides containing cysteines were selected, and oxidation status (percentage) was calculated and further statistically analyzed.

2.3. Cell culture

For the redox-switch assay, human neuroblastoma cells (SH-SY5Y) were used. Cells were maintained in a 1:1 mix of minimal essential medium (ATCC, Wesel, Germany) and F-12 Nutrient Mix (Gibco, Carlsbad, CA) containing 15% fetal calf serum, 1% glutamine, 1% nonessential amino acid mix, and 1% penicillin–streptomycin at 5% CO_2 and 37°C, and passaged once a week. Cells were cultured for 3 days before stimulation with 100 μM H_2O_2 for 5 minutes.[45]

In addition, murine neuroblastoma cells (Neuro-2a) were used for transfection of Rab7 plasmids. Cells were cultivated in advanced DMEM containing 10% fetal calf serum (FCS), 1% glutamine, and 1% penicillin–streptomycin at 5% CO_2 and 37°C and passaged twice a week. Transfection of cells was performed as described below.

2.4. Switch assay

Detection of oxidized thiols in the Rab7 protein was performed according to previous published methods.[4,15,16,78] SH-SY5Y cells were stimulated with 100 μM H_2O_2 as described above and homogenized in homogenization buffer (50 mM Tris, pH 7.4, 150 mM NaCl, 25 mM NEM, 2% Triton-X, protease-inhibitor mix)

and incubated for 5 minutes at room temperature (RT), followed by incubation for 5 minutes on ice. Cells were centrifuged at 16,000*g* and 4°C for 20 minutes, and the supernatant was precipitated with ice-cold acetone. Pellets were solubilized in solubilization buffer (50 mM Tris, pH 7.4, 150 mM NaCl, 2% Triton-X, protease-inhibitor mix) and reduced with TCEP (final concentration 2 mM) for 1 hour at 37°C. Cy5-labeled maleimide was added, and samples and were incubated for another hour at 37°C. Samples were then precipitated with ice-cold acetone and solubilized again in solubilization buffer. Rab7 protein was immunoprecipitated with rabbit anti-Rab7 (1:500; Sigma-Aldrich # R4779) and protein A/G agarose beads (Santa Cruz Biotechnology, Dallas, TX). Immunoprecipitated proteins were separated with SDS polyacrylamide gel electrophoresis and blotted onto a nitrocellulose membrane. Cy5-labeled (originally oxidized) proteins were detected using an Odyssey Infrared Imaging System (LI-COR Bioscience, Bad Homburg, Germany). Afterwards, membranes were blocked in blocking buffer (Odyssey blocking buffer, diluted 1:1 in PBS; LI-COR Bioscience) for 1 hour at RT and then incubated with rabbit anti-Rab7 (1:500; Cell Signaling Technology, Cambridge, UK, # 93679) dissolved in blocking buffer containing 0.1% Tween-20 overnight at 4°C, followed by incubation with a secondary antibody for 1 hour at RT. Detection of Rab7 total protein was again performed using the Odyssey Infrared Imaging System, and quantification of band densities was done using NIH ImageJ software.

2.5. Cloning of the Rab7 "redox-dead" plasmid

Cloning of the a redox-insensitive Rab7 construct, further termed as "redox-dead," was performed using the Q5-Site-Directed Mutagenesis Kit (New England Biolabs, Frankfurt, Germany) according to the manufacturer's instructions. Primers were designed using the NEBase Exchanger v1.2.1 (Q5SDM_fwd 5′-agg tgc aga cag cag tgt tct ggt att tg -3′, Q5SDM_rev 5′- ctg tag aag gcc aca ccg -3′) to exchange nucleotides coding for the 2 cysteines in position 83 and 84 of Rab7 (NCBI accession Number CAJ18560.1) to serine. Plasmid containing green fluorescent protein (GFP)-rab7 wildtype (WT) (clone 12605; Addgene Inc, Cambridge, MA) was used as template DNA. PCR amplification, ligation, and transformation were performed according to the manufacturer's protocol. NEB 5-alpha competent *E.coli* containing the Rab7 redox-dead plasmid were plated on kanamycin-containing agar plates. Plasmid isolation of selected clones was performed using the QIAprep Spin Miniprep Kit. Sequence verification was performed by LGC Genomics (Berlin, Germany).

Transfection of plasmids was performed using FuGENEHD Transfection Reagent (Promega, Mannheim, Germany) according to the manufacturer's protocol. Neuro-2a cells were seeded into 12-well or 6-cm dishes at a density of 4×10^3 and 4×10^5, respectively. Transfection was performed immediately after seeding using a ratio of 5:2 of FuGENE transfection reagent and plasmid DNA.

2.6. Rab7 activity assay

Activity status of Rab7 constructs was assessed using an Rab7 activation assay kit (NewEast Bioscience, Malvern, PA). The assay was performed according to the manufacturer's instructions. Briefly, Neuro-2a cells were transfected with Rab7-WT or Rab7 redox-dead constructs and cultured for 2 days. Cells were then lysed in assay buffer, centrifuged, and supernatants were loaded either with GTP or Guanosine-5′-diphosphate (GDP) to stimulate Rab7. Active/GTP-bound Rab7 was then immunoprecipitated and detected by immunoblot. Values were calculated to the respective GDP loaded control.

2.7. Real-time reverse transcription PCR

Total RNA from the lumbar spinal cord (L4-L5), lumbar DRG (dorsal root ganglia) (L4-L5), and the sciatic nerve was extracted under RNase-free conditions using TRI-reagent (Sigma-Aldrich) or the RNAqueous Micro Kit (Ambion/Life Technologies, Darmstadt, Germany). Reverse transcription was performed using a First Strand cDNA Synthesis Kit (Thermo Scientific, Waltham, MA) according to the manufacturer's instructions. Quantitative real-time RT-PCR was performed with an ABI Prism 7500 Sequence Detection System (Applied Biosystems/Life Technologies) using gene-specific primer pairs for murine Rab7 (fwd 5′-gga aga aag tgt tgc tga agg -3′, rev 5′-tgt ggc ttt gta ctg gtt act g-3′) and GAPDH (fwd 5′-caa tgt gtc cgt gga tct -3′, rev 5′-gtc ctc agt gta gcc caa gat g-3′). Reactions were performed in duplicate or triplicate by incubating for 10 minutes at 95°C, followed by 40 cycles of 15 seconds at 95°C and 1 minute at 60°C, including water controls to ensure specificity. Relative gene expression levels were calculated using the comparative $2^{-\Delta\Delta Ct}$ method and normalized to GAPDH.

2.8. Immunohistochemistry

Immunofluorescent staining of lumbar spinal cord and DRG slices (L4-L5) was performed as described previously.[22,35] Briefly, cryostat sections were permeabilized, blocked in 10% normal goat or donkey serum and 3% bovine serum albumin in PBS, and incubated with primary antibodies overnight at 4°C. The following primary antibodies were used: rabbit anti-Rab7 (1:200, Proteintech # 55,469-1-AP; Manchester, United Kingdom), mouse anti–neurofilament 200 (NF200; 1:1000; clone N52; Sigma-Aldrich, St. Louis, MO), and mouse anti–calcitonin gene-related peptide (1:200; Abcam # ab 81887). After rinsing in PBS, slides were incubated with secondary antibodies conjugated with Alexa Fluor 488, Alexa Fluor 555 (Invitrogen/Life Technologies), or Cy3 (Sigma-Aldrich) for 2 hours at RT. For staining with *Griffonia simplicifolia* isolectin B4 (IB4), sections were incubated with Alexa Fluor 488-conjugated IB4 (10 μg/mL in 0.1 mM $CaCl_2$, 0.1 mM $MgCl_2$, 0.1 mM $MnCl_2$, and 0.2% Triton in PBS; Invitrogen/Life Technologies) for 2 hours at RT. Finally, lipofuscin-like autofluorescence was reduced by incubating in 0.06% Sudan black B in 70% ethanol for 5 minutes,[67,68] and slides were rinsed in PBS and cover slipped in Fluoromount G (Southern Biotech, Birmingham, England). Images were taken using a Nikon Eclipse Ni-U microscope (Nikon, Japan) and a monochrome DS-Qi2 camera (Nikon, Minato, Tokyo, Japan). Final adjustment of contrast and intensity was performed using Adobe Photoshop software.

2.9. In situ hybridization

Mice were killed by CO_2 and intracardially perfused with 4% formaldehyde (PFA) in PBS for 5 minutes. Dorsal root ganglia were dissected and postfixed in the same fixative for 10 minutes. Tissue was then incubated in 20% sucrose in PBS overnight, embedded in Tissue Tek mounting media (Sakura Finetek, Alphen aan den Rijn, Netherlends), and cryostat sections were cut at a thickness of 16 μm. In situ hybridization (ISH) was performed using an Affymetrix QuantiGene ViewRNA Tissue Assay in which target mRNA signals appear as puncta in microscopy.[58,72] Experiments were performed according to the instructions of the manufacture and included extensive washing

steps in PBS. Briefly, sections were fixed in 4% PFA overnight, dehydrated for 10 minutes in a 50%, 70%, and 100% ethanol series, dried for 30 minutes at 60°C in a ThermoBrite slide processing system (Abbott Molecular, Des Plaines, IL), and digested with the Protease QF Mix for 20 minutes. Then sections were fixed again in 4% PFA for 5 minutes and hybridized overnight at 40°C (ThermoBrite) with an approximately 600 nucleotides spanning type 1 probe set designed by Affymetrix to mouse Rab7 (NCBI accession number NM_009005, catalog # VB1-20408). In control experiments, a scramble probe (catalog # VF1-17155) was used. Sections were then consecutively incubated with PreAmplifier Mix QT, Amplifier Mix QT, an alkaline phosphatase–labeled probe against the Amplifier, AP Enhancer Solution, and Fast Red Substrate (Cy3 fluorescence). Finally, sections were coverslipped with Fluoromount-G (Southern Biotech) or further processed for subsequent immunohistochemistry.

In ISH experiments combined with immunohistochemistry, hybridization of Rab7 was performed as described above. Sections were then blocked in 10% NGS and 3% bovine serum albumin in PBS-Triton-X 100 for 1 hour and incubated with primary antibodies overnight. The following antibodies were used: rabbit anti-NF200 (Sigma-Aldrich, # N4142) and mouse anti-peripherin (Chemicon, # MAB1527). After rinsing in PBS, slides were incubated with secondary antibodies conjugated with Alexa Fluor 488 or Cy5 (Invitrogen/Life Technologies) for 2 hours at RT. Lipofuscin-like autofluorescence was reduced as described above, and slides were coverslipped with VECTASHIELD HardSet Antifade Mounting Medium with DAPI (Vector Laboratories, Burlingame, VT, # H-1500). Images were taken and adjusted as described above.

2.10. Cell counting

To analyze the distribution of Rab7 mRNA in DRG neurons, only Rab7-positive profiles with a clear nucleus were analyzed. The percentage of all DRG neurons (visualized by the autofluorescence of DRG neurons) positive for Rab7 and of Rab7-positive DRG neurons expressing peripherin or NF200 was calculated. In total, >2000 DRG neurons of 6 animals (at least 150 cells per animal) were counted.

To analyze DRG neuron subpopulations of Adv-Rab7$^{+/-}$ mice, the percentage of neurons positive for marker (IB4, NF200) was calculated from 4 animals per genotype and 2 sections per animal (>2000 cells per genotype). Only DRG neurons showing staining clearly above background were included. Sections were chosen randomly with at least 70 μm apart.

2.11. Western blot

Lumbar (L4-L5) spinal cords, the dorsal part of lumbar spinal cords, lumbar DRG, and sciatic nerves were rapidly dissected, frozen in liquid nitrogen, and stored at −80°C until use. Samples were homogenized in PhosphoSafe buffer (Novagen/Merck Millipore, Darmstadt, Germany) combined with a protease inhibitor cocktail (Complete Mini; Roche Diagnostics, Mannheim, Germany) and centrifuged at 14,000*g* for 1 hour. Extracted proteins (20 μg per lane) were separated by SDS polyacrylamide gel electrophoresis and blotted onto a nitrocellulose membrane. Membranes were blocked in blocking buffer (Odyssey blocking buffer, diluted 1:1 in PBS; LI-COR Bioscience) for 1 hour at RT and then incubated with rabbit anti-Rab7 (1:200; Cell Signaling # 93679, Danvers, MA) or mouse anti-GAPDH (1:2000; Ambion # AM4300) dissolved in blocking buffer containing 0.1% Tween-20 overnight at 4°C. After incubation with secondary antibodies for 1 hour at RT, proteins were detected using an Odyssey Infrared Imaging System (LI-COR Bioscience). Quantification of band densities was performed using NIH ImageJ software.

2.12. Behavioral tests

Behavioral studies were performed by a blinded observer. Experiments were performed using littermate mice of either sex at the age of 7 to 12 weeks.

2.12.1. Rotarod test

A rotarod treadmill for mice (Ugo Basile, Varese, Italy) was used to assess motor coordination, running at a constant rotating speed of 12 rpm. After several training sessions, fall-off latencies from 3 to 5 tests were averaged. The cut-off time was set at 120 seconds.

2.12.2. Hot-plate and cold-plate test

Mice were placed on a heated or cooled metal plate surrounded by a plexiglas cylinder (Hot/Cold Plate; Ugo Basile, Monvalle, Italy). For the hot-plate test, the latency time between placing and the first nociceptive reaction (shaking or licking) of a hind paw was recorded. Experiments were performed at temperatures of 50, 52, and 54°C with cut-off times of 60, 40 and 20 seconds, respectively, to prevent tissue damage. In the cold-plate test, the metal plate was cooled down at 0°C, and the number of reactions over a period of 5 minutes was counted. Hind paw withdrawal, hind paw licking and jumping were considered as a reaction.[41]

2.12.3. Dynamic plantar test

Mechanical sensitivity of the hind paw was analyzed using a dynamic plantar aesthesiometer (Ugo Basile). The device pushes a thin probe (0.5 mm diameter) with increasing force through a wire-gated floor against the plantar surface of the paw from beneath. When the animal withdraws the paw, the device automatically stops and records the latency time, which is the time from when the probe touched the paw to when the animal withdrew the paw. The force was increased from 0 to 5 g within 10 seconds (0.5 g/s ramp) and then held at 5 g for an additional 10 seconds. Paw withdrawal latencies were calculated as the mean of 4 to 6 measurements with at least 20 seconds in between.[35,46,67]

2.12.4. Zymosan-induced hyperalgesia

Fifteen microliters of a zymosan A suspension (5 mg/mL in 0.1 M PBS, pH 7.4; Sigma-Aldrich) was injected into the plantar subcutaneous surface of a hind paw (Meller and Gebhart, 1997). Mechanical sensitivity of the affected hind paw was measured using the dynamic plantar test as described above. Thermal hypersensitivity was assessed using a plantar test (Hargreaves Apparatus; Ugo Basile). Infrared light beam intensity was set to 25, which resulted in paw withdrawal latencies of 8 to 10 seconds for baseline measurements.

2.12.5. Reactive oxygen species–induced pain behavior

The ROS donor, tert-butyl hydroperoxide (TBHP; 2.2 μmol), dissolved in 20 μL saline, was injected subcutaneously into the dorsal surface of a hind paw and the time spent licking the TBHP-injected paw was measured over a period of 10 minutes. The TBHP dose was selected on the basis of previous studies.[34,47]

2.13. Statistics

SPSS (IBM) or GraphPad Prism 5 (GraphPad) software was used for statistical analyses. For paired comparisons and multiple comparisons, the unpaired, 2-tailed Student *t* test or 2-way analysis of variance was used, the latter followed by *t* tests using a Bonferroni correction. Rotarod fall-off latencies were analyzed with the Mann–Whitney *U* test and are presented as medians and interquartile ranges. Other data are expressed as the mean ± SEM. For all tests, a probability value $P < 0.05$ was accepted as statistically significant. Number of mice and replicates are given in the figure legends.

3. Results

3.1. Identification of reactive oxygen species targets in chronic pain processing

To identify pain-relevant ROS targets, we performed the well-characterized in vivo model of zymosan-evoked hind paw inflammation in mice.[22,33,48,52] Eight hours after the zymosan injection (ie, at a time point when mechanical hyperalgesia was pronounced, as indicated by a drop in paw withdrawal latencies, **Fig. 1A**), the lumbar spinal cord was removed and analyzed using the OxICAT thiol-trapping technique,[42] which allows for screening redox-modulated thiol groups in proteins. As shown in **Table 1**, we identified 10 proteins that were significantly redox modulated in zymosan-injected mice as compared to naive control mice (≥2 fold changes in the redox-state; $P < 0.05$; n = 3-4 animals per group). Of interest, the protein found to be most strongly oxidized after zymosan injection was the small GTPase Rab7 (**Fig. 1B**). Moreover, the sequence detected by the OxICAT screen is highly conserved among species (**Fig. 1C**). Previous studies suggest a contribution of Rab7 to pain processing;[55,66,77]

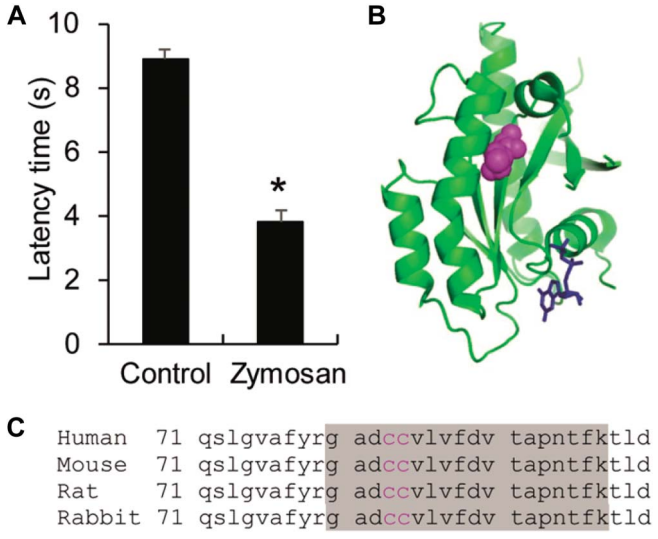

Figure 1. An OxICAT screen detects Rab7 redox modifications in the spinal cord after zymosan injection into a hind paw. (A) Mechanical hyperalgesia 8 hours after the zymosan injection, as indicated by a drop in withdrawal latencies on mechanical hind paw stimulation using a Dynamic Plantar Aesthesiometer (n = 4, *$P < 0.05$). This time point was chosen for OxICAT analysis of spinal cord tissue. Identified proteins are presented in Table 1. (B) Positions of redox modifications in the Rab7 peptide. The structure of GDP-bound (blue) Rab7 (green) from rat [PDB database: 1vg1[61]] was used to visualize redox-modified cysteines (magenta). (C) Alignment of Rab7 protein sequence of amino acids 71 to 100 in different species. The gray marked sequence (with redox-sensitive cysteines in positions 83 and 84) was detected by the OxICAT screen. This Rab7 protein sequence is highly conserved among species.

Table 1

Redox-modulated proteins identified in the OxICAT screen.

Symbol	Protein ID	Sequence	Fold increase	*P*
Lin7C	22,343	VLQSEFcNAVR	−31.32	0.021
Rpl4	67,891	YAlcSALAASALPALVmSK	2.53	0.042
Cltc	67,300	mEGNAEESTLFcFAVR	2.56	0.013
Ppp3cb	19,056	HLTEYFTFKQEcK	2.72	0.035
Tkt	21,881	QAFTDVATGSLGQGLGAAcGMAYTGK	3.21	0.015
Plec	18,810	FLEGTSclAGVFVDATK	3.52	0.040
Vwa5a	67,776	cFSFGIGQGASTSLIK	3.68	0.048
Padi2	18,600	LLMASTSAcYQLFR	5.04	0.006
Rhog	56,212	TcLLIcYTTNAFPK	19.73	0.034
Rab7	19,349	GADccVLVFDVTAPNTFK	23.03	0.019

however, its possible function as a pain-relevant ROS target has not been investigated yet. We therefore focused on Rab7 for the remainder of our study.

3.2. Rab7 is a reactive oxygen species target in vitro

To confirm that Rab7 may serve as a target for ROS-based signaling, we performed a modified switch assay in which oxidized thiols are labeled with maleimide-Cy5, and the protein of interest is then enriched by immunoprecipitation.[15,16,78] As shown in **Figure 2**, stimulation of SH-SY5Y neuroblastoma cells with 100 μM H_2O_2 resulted in increased oxidation of Rab7 as indicated by increased Rab7-Cy5 labeling. These in vitro data support our observation that Rab7 is sensitive to ROS-dependent oxidation.

3.3. Rab7 expression in the spinal cord and dorsal root ganglia

We then investigated the distribution of Rab7 in the murine spinal cord using immunostaining. We found Rab7 expression to be enriched in the superficial laminae of the dorsal horn and in distinct neurons of the ventral horn (**Fig. 3A**). Double-labeling experiments revealed Rab7 expression in calcitonin gene–related peptide- and isolectin B4 (IB4)-positive fibers (**Fig. 3B, C**), which are markers for peptidergic and non–peptidergic unmyelinated nociceptors, respectively. Co-localization was also detected for Rab7 and NF200 (**Fig. 3D**), a marker of large myelinated primary afferents. Specificity of anti-Rab7 was confirmed by the reduced immunoreactivity in the spinal cord of mice lacking Rab7 in sensory neurons (Adv-Rab7$^{-/-}$, **Fig. 3E**). These data suggest that Rab7 is enriched in central sensory neuron terminals and in motoneurons of the spinal cord of naive mice.

We next analyzed the Rab7 localization in DRG. As immunostaining experiments using various protocols failed to detect specific Rab7 immunoreactivity in DRG, we performed fluorescent ISH of Rab7 mRNA. We found Rab7 to be expressed in the majority of DRG neurons (89.2% ± 4.3%; **Fig. 4A**). As expected, no hybridization signals were detected using a scramble control probe (**Fig. 4B**). To further characterize the localization of Rab7 in DRG neuron subpopulations, we combined ISH of Rab7 mRNA with immunostaining for the marker peripherin and NF200, which stain unmyelinated and myelinated DRG neurons, respectively. We found that

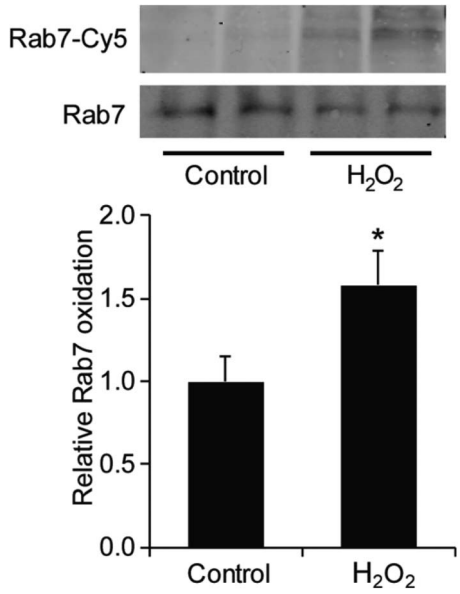

Figure 2. Validation of Rab7 oxidation in vitro. SH-SY5Y cells were stimulated with 100 μM H_2O_2 for 5 minutes. A redox-switch assay using maleimide-Cy5–labeled Rab7 revealed increased Rab7 oxidation (indicated by increased Rab7-Cy5 protein) after H_2O_2 stimulation (n = 8, $^*P < 0.05$).

48.4% ± 5.1% of Rab7-positive neurons expressed peripherin (**Fig. 4C**), whereas 42.0% ± 3.4% of Rab7-positive neurons were also positive for NF200 (**Fig. 4D**). These data suggest that Rab7 is expressed in both unmyelinated small C fiber neurons and large myelinated DRG neurons of naive mice.

We then performed Western blot experiments to analyze whether Rab7 expression in DRG and the dorsal horn of the spinal cord is altered during zymosan-induced hind paw inflammation. Of interest, we found Rab7 expression to be significantly increased in ipsilateral DRG 4 and 8 hours after the zymosan injection (**Fig. 5A**), whereas Rab7 expression was significantly reduced in the ipsilateral dorsal horn of the spinal cord (**Fig. 5B**). Quantitative real-time RT-PCR analyses revealed that Rab7 mRNA was not upregulated in ipsilateral DRG 6 hours after the zymosan injection (relative Rab7 mRNA expression: naive mice, 1.00 ± 0.06; zymosan-injected mice, 1.15 ± 0.17; $P = 0.48$; n = 3). Hence, these data point to a zymosan-induced translocation of Rab7 protein to the somata of DRG neurons. This assumption is supported by an earlier study in which Rab7 translocation to perinuclear lysosome compartments of DRG neurons was observed during diabetic neuropathy in rats.[55] Altogether, these data point to a contribution of Rab7 to pain processing.

3.4. Rab7 knockdown mice display normal basal sensitivity

To characterize the function of Rab7 in sensory neurons in vivo, we crossed mice carrying the floxed exon 1 of the *Rab7* gene[63] with Advillin-Cre mice,[21,79] to obtain mice lacking Rab7 specifically in primary afferent neurons. Unexpectedly, we only obtained a relatively small proportion (8.9%) of homozygous mutant mice (Adv-Rab7$^{-/-}$) in the offspring suggesting that homozygous mutant mice already die within the late prenatal period. This observation is in accordance with a previous study in Drosophila in which a complete loss of Rab7 severely impaired pupal development and with the observation that mutations in the *Rab7* gene caused defects in sensory neuron axon growth, branching, and path finding in a zebrafish model.[7,59] We therefore used heterozygous mutant mice (Adv-Cre; Rab7$^{+/fl}$; referred to as Adv-Rab7$^{+/-}$) in our behavioral studies.

Quantitative real-time RT-PCR analyses revealed a reduced Rab7 mRNA expression in DRG of Adv-Rab7$^{+/-}$ mice

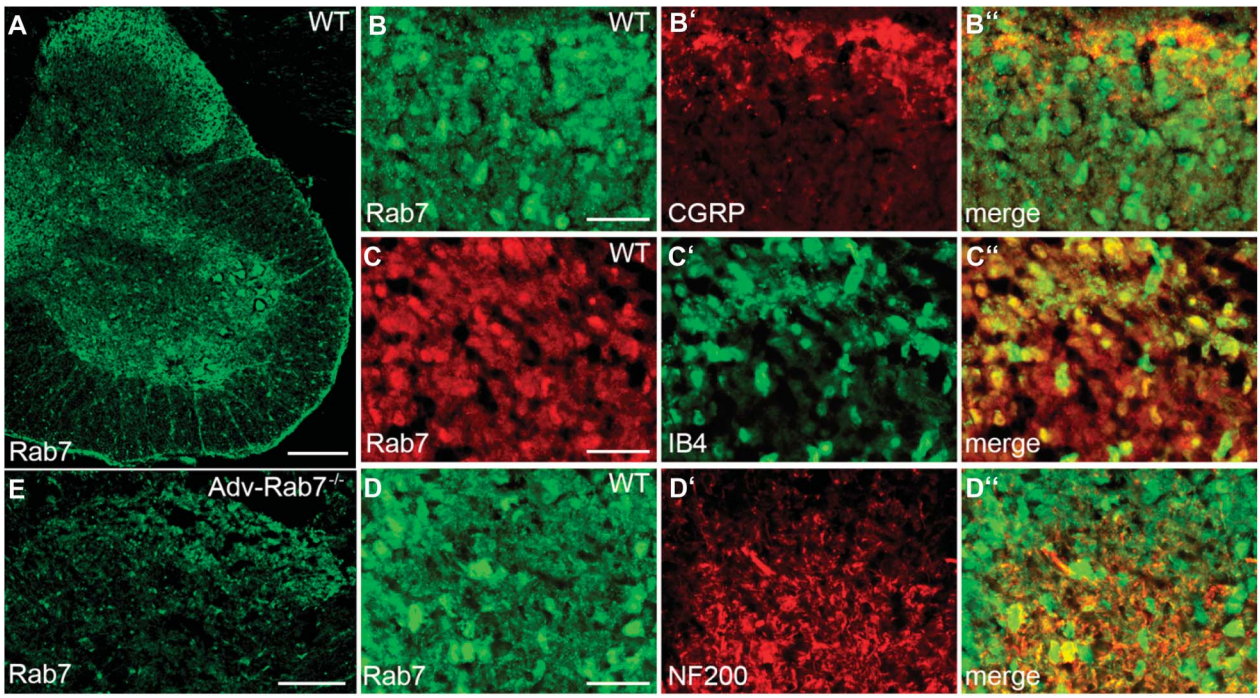

Figure 3. Localization of Rab7 in the spinal cord. (A) Rab7 expression is enriched in the superficial layer of the dorsal horn and in some ventral horn neurons. (B-D) Rab7 co-localizes with CGRP- (B) and IB4- (C) positive unmyelinated nociceptors. There is also some co-localization with NF200 (D), a marker for large myelinated neurons. (E) Rab7 expression in the dorsal horn is reduced in Adv-Rab7$^{-/-}$ mice, in which Rab7 is selectively knocked out in sensory neurons (scale bars: A = 200 μm, B-D = 25 μm, E = 100 μm). CGRP, calcitonin gene–related peptide.

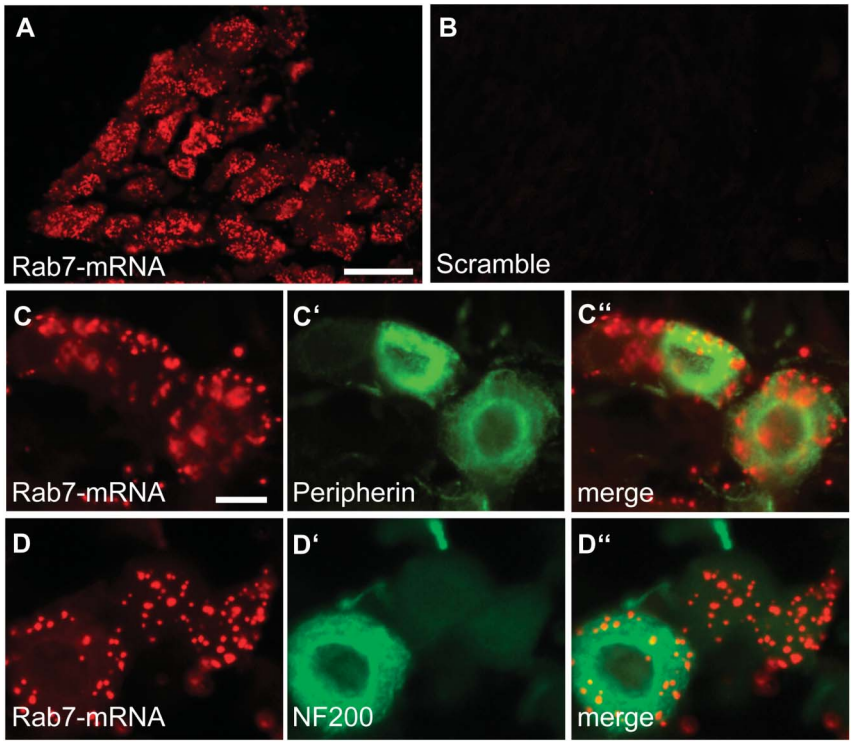

Figure 4. Localization of Rab7 in DRG. (A) Fluorescent in situ hybridization detected Rab7 mRNA in the majority of DRG neurons. (B) No hybridization signal was detected using scramble (negative) control. (C, D) Rab7 mRNA is expressed in peripherin-positive (C) and NF200-positive (D) DRG neurons. Scale bars: A = 50 μm, C = 10 μm. DRG, dorsal root ganglia; mRNA, messenger RNA.

compared with control mice, whereas mRNA expression levels in the spinal cord, the kidney, and the heart were similar between groups (**Fig. 6A**). At the protein level, Rab7 expression was reduced in tissue lysates of the spinal cord, DRG, and the sciatic nerve of Adv-Rab7$^{+/-}$ mice (**Fig. 6B**). Moreover, the proportion of DRG neurons positive for IB4 and neurofilament 200 (NF200) was similar between genotypes (**Fig. 6C**). Hence, Rab7 expression is moderately reduced at sites of Advillin-Cre–mediated recombination in Adv-Rab7$^{+/-}$ mice.

We next investigated nociceptive behavior of Adv-Rab7$^{+/-}$ in male and female mice,[18,54] but no significant sex effects were detected in any assay. Motor functions were not impaired in

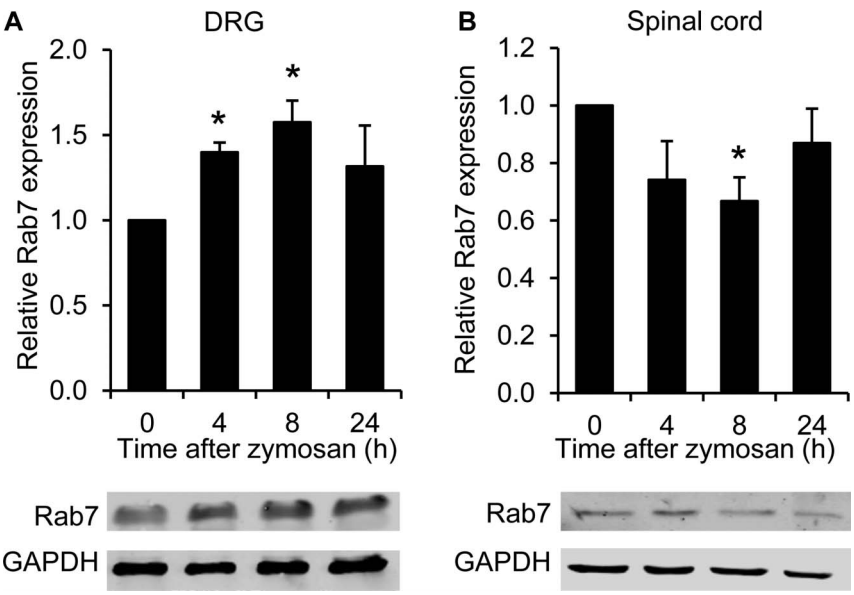

Figure 5. Rab7 expression after zymosan-induced hind paw inflammation. (A) Western blot analyses detected increased Rab7 protein levels in DRG 4 hours and 8 hours after zymosan injection into a hind paw. (B) In contrast, Rab7 protein levels in the ipsilateral dorsal horn of the spinal cord were significantly decreased 8 hours after the zymosan injection. n = 3 to 4, *$P < 0.05$. DRG, dorsal root ganglia.

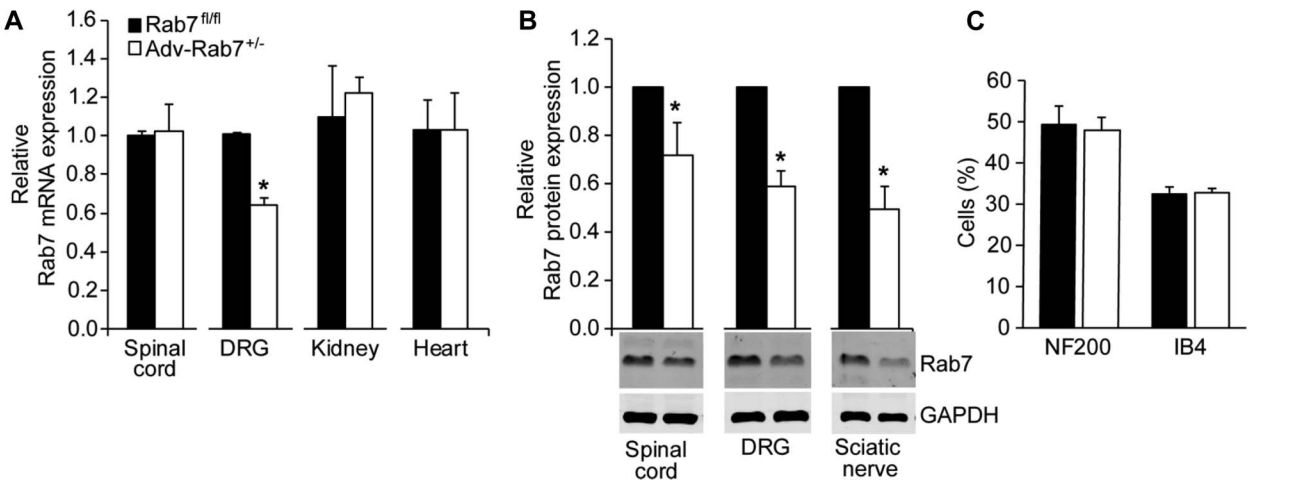

Figure 6. Basal characterization of Rab7-knockdown mice. (A) Quantitative RT-PCR experiments revealed that Rab7 mRNA levels are specifically reduced in DRG of Adv-Rab7$^{+/-}$ mice compared with Rab7$^{fl/fl}$ mice, whereas Rab7 mRNA expression is not affected in the spinal cord, the kidney, or the heart (n = 3-4, *$P < 0.05$). (B) Western blot experiments demonstrated that Rab7 protein expression is reduced in the spinal cord, DRG, and the sciatic nerve of Adv-Rab7$^{+/-}$ mice compared with Rab7$^{fl/fl}$ mice (n = 3-5, *$P < 0.05$). (C) Quantification of DRG neuron populations in Adv-Rab7$^{+/-}$ and Rab7$^{fl/fl}$ mice. The percentage of IB4- and NF200-positive DRG neurons is similar between genotypes (n = 4). DRG, dorsal root ganglia; mRNA, messenger RNA; RT-PCR, reverse transcription PCR.

Adv-Rab7$^{+/-}$ mice, as analyzed in the rotarod test (median fall-off latencies Rab7$^{fl/fl}$: 120 seconds [interquartile range: 99.3-120 seconds], Adv-Rab7$^{+/-}$: 120 seconds [interquartile range: 117.8-120 seconds]; $P = 0.497$; n = 10–12). Acute nociceptive behaviors on a 50 to 54°C hot plate (**Fig. 7A**) or a 0°C cold plate (**Fig. 7B**) were similar between genotypes. Moreover, basal sensitivity to mechanical stimuli was not affected by the Rab7 knockdown (**Fig. 7C**). These data suggest that the immediate responses to acute nociceptive thermal and mechanical stimuli are intact in Adv-Rab7$^{+/-}$ mice.

3.5. Inflammatory and reactive oxygen species–induced pain behavior is reduced in Rab7 knockdown mice

We next assessed the behavior of Adv-Rab7$^{+/-}$ and control mice in the zymosan model of inflammatory pain, in which Rab7 oxidation was detected (**Fig. 1**). Injection of zymosan into a hind paw resulted in mechanical hypersensitivity in both genotypes. Notably, the extent of hypersensitivity was significantly lower in Adv-Rab7$^{+/-}$ mice as compared to control littermates (**Fig. 8A**). In contrast to mechanical hypersensitivity, thermal hypersensitivity was not significantly affected by the Rab7 knockdown (**Fig. 8B**). These data suggest that Rab7 functionally contributes to mechanical, but not thermal, hypersensitivity during the processing of inflammatory pain.

We then investigated the pain behavior in response to ROS delivery. For this purpose, we injected the ROS donor TBHP (2.2 μmol) into a hind paw and observed the induced paw licking behavior over a period of 10 minutes. As shown in **Figure 8C**, Adv-Rab7$^{+/-}$ mice demonstrated significantly less paw licking compared with control littermates, suggesting that Rab7 is a target of ROS-induced pain sensitization in vivo. Altogether, these behavioral data in combination with our OxICAT screen indicate functional contribution of Rab7 oxidation to inflammatory pain processing.

3.6. Redox modifications affect Rab7 activity in vitro

To assess the functional implications of Rab7 oxidation, we transfected Neuro-2a neuroblastoma cells with Rab7-WT or an Rab7 redox-dead construct, in which the redox-sensitive thiol residues of Rab7 were each replaced by serine (**Fig. 9A**). In both constructs, Rab7 was tagged to GFP resulting in an enhanced molecular weight (50 kDa) compared with native Rab7 (23 kDa) as detected by Western Blot (**Fig. 9B**), allowing us to distinguish between native and transfected Rab7. In the transfected cells, we determined Rab7 activity using an Rab7 activation assay kit. Surprisingly, we found that after GTP loading, Rab7 activity was higher in cells transfected with Rab7 redox-dead cells (**Fig. 9C**). We further assessed subcellular localization of native and mutant Rab7 by immunostaining, but there was no obvious difference (**Fig. 9D**). Hence, oxidation of Rab7 suppresses its GTP-binding activity suggesting that the observed oxidation in the spinal cord in the context of inflammatory pain processing is associated with reduced GTPase activity.

4. Discussion

In this study, we show that redox-mediated posttranslational protein modifications contribute to inflammatory pain hypersensitivity. In an OxICAT screen, we identified Rab7, which is highly expressed in sensory neurons and their central terminals in the superficial laminae of the spinal cord, as an oxidized target during pain processing. We further show that the activity of Rab7 was altered in vitro in a redox-dependent manner and that heterozygous Rab7 deficiency reduced inflammatory and ROS-induced pain behavior.

In the last few years, our understanding of redox signaling has increased dramatically. Although ROS were initially considered as harmful agents that attack proteins, lipids, or nucleic acids, it is now clear that they serve as signaling molecules that modify protein activity at a posttranscriptional level. Oxidative modifications may alter the functions of the respective targeted cysteine residues, and this may result in changes in enzyme activity, binding properties, stability, or localization. Redox-dependent protein modifications include the formation of intra- or inter-protein disulfides, S-sulfenation, S-sulfination, S-sulfonation, S-nitrosylation, S-sulfhydration, or S-sulfenamidation.[29,44,64] Advances in biochemical and

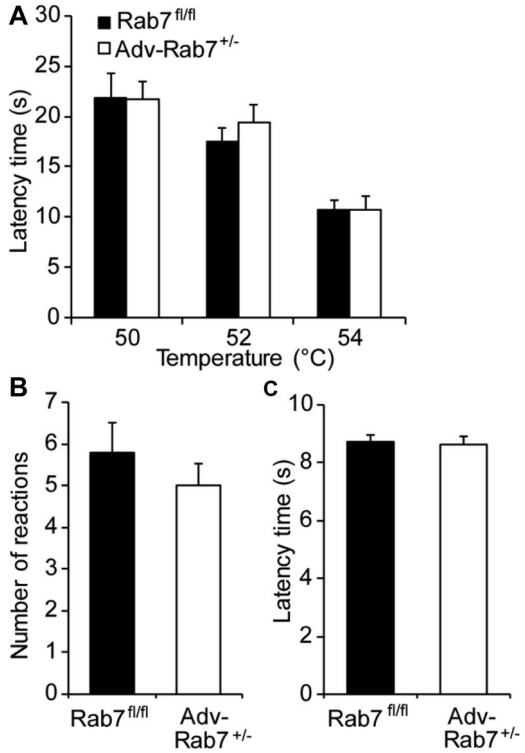

Figure 7. Acute nociceptive pain is normal in Rab7-knockdown mice. Adv-Rab7$^{+/-}$ mice displayed normal sensitivity to acute thermal stimuli on a 50 to 54°C hot plate (A; n = 12-13) and a 0°C cold plate (B; n = 8-10), and after mechanical stimulation of the hind paw using a Dynamic Plantar Aesthesiometer (C; n = 16).

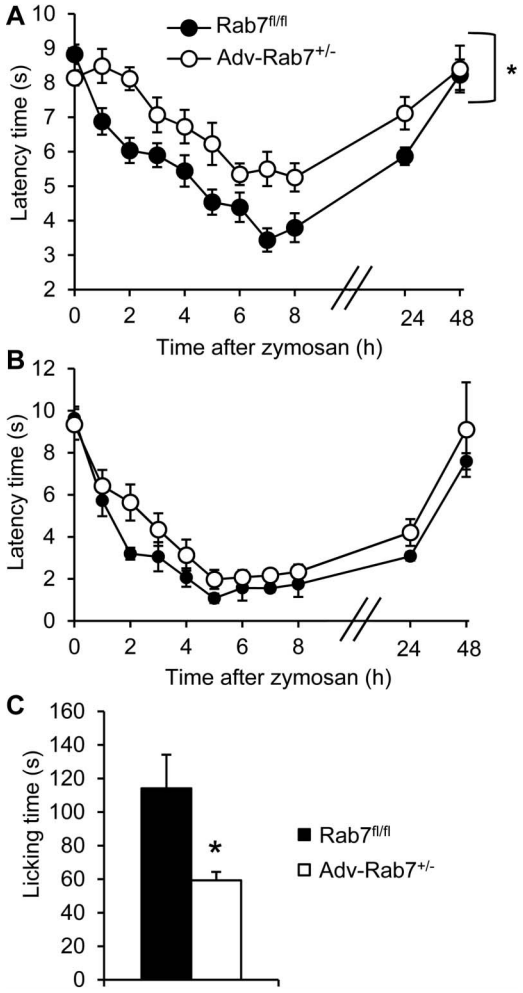

Figure 8. Inflammatory and ROS-induced pain behavior is reduced in Rab7-knockdown mice. (A) Mechanical hypersensitivity after zymosan injection into a hind paw was significantly reduced in Adv-Rab7$^{+/-}$ mice as compared to Rab7$^{fl/fl}$ mice. Paw withdrawal latencies were determined using a Dynamic Plantar Aesthesiometer (n = 8, *$P < 0.05$). (B) Thermal hypersensitivity after zymosan injection was not significantly affected in Adv-Rab7$^{+/-}$ mice. Paw withdrawal latencies were determined using a Hargreaves apparatus (n = 6, $P = 0.374$). (C) Paw licking after injection of the ROS-donor TBHP (2.2 μmol) into a hind paw was significantly reduced in Adv-Rab7$^{+/-}$ compared with Rab7$^{fl/fl}$ mice (n = 5-7, *$P < 0.05$). ROS, reactive oxygen species; TBHP, tert-butyl hydroperoxide.

molecular biology methods have allowed the identification and quantification of redox-modified proteins. These methods often make use of different labeling and trapping of the redox status of protein residues that stabilize the relatively labile oxidation-modified cysteines with stable alkylated tags which can then be detected by electrophoresis, enzyme-linked immunosorbent assay, or mass spectrometry (MS) analysis.[23,64] Although the OxICAT-labeling technique we used here revealed several redox-modified proteins, the method has its limitations. For example, higher oxidation states of the thiolate ion such as S-sulfination or S-sulfonation are not detected by OxICAT. Furthermore, the method preferentially detects abundant proteins. One could argue that the time point we chose (ie, 8 hours after zymosan injection) was associated with an increased protein expression that resulted in false-positive OxICAT hits. However, we did observe significant zymosan-induced Rab7 downregulation in the spinal cord (**Fig. 5B**), suggesting that the changes we detected in the OxICAT screen were due to oxidation and not upregulation of Rab7 protein. We only analyzed proteins which were reliably detected in at least 3 of 4 samples. Thus, less abundant proteins, which were not detected in all samples, might also be involved in redox signaling in the dorsal horn.

Several studies suggest a function of ROS as signaling molecules in various pain states. For example, administration of ROS scavengers and antioxidants reduced nociceptive responses in inflammatory pain models,[19,39,70] and impaired ROS production in knockout mice was associated with reduced pain hypersensitivity.[26,27,32,35,38,43] However, so far, only a few redox targets have been found at sites of nociceptive signal transduction. The small GTPase Rab7, which we identified as a redox target in the nociceptive system, is an essential protein, regulating endosomal maturation and controlling various steps in membrane trafficking.[75,76] Mutations in the *Rab7* gene that result in increased Rab7 activity are associated with the Charcot–Marie–Tooth type 2B (CMT2B) disease, a peripheral neuropathy that is characterized by sensory loss, near-normal nerve conduction velocities, foot deformations, and a high frequency of ulcers and infections.[3,8,17] In sensory neurons, Rab7 plays an essential role in axonal retrograde transport, acting in a sequential manner together with Rab5, thus controlling trafficking and neurite outgrowth.[6,9,11,77] Of interest, an earlier study showed that Rab7 co-localizes with the ROS-producing enzyme, tartrate-resistant acid phosphatase in alveolar macrophages.[60] Moreover, infections with the human hepatitis virus strongly depend on Rab7-dependent endosomal transport which involves alterations in the redox state of the disulfide-bound envelope proteins of the virus.[49] These studies imply that

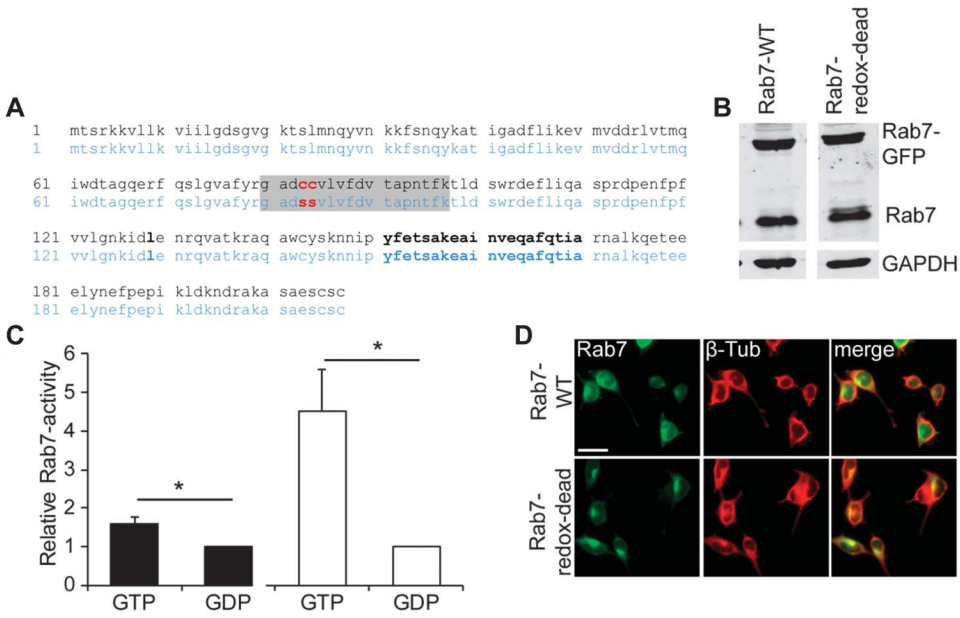

Figure 9. Cloning of an Rab7 redox-dead construct. (A) Sequence of Rab7-WT (black) and Rab7 redox-dead (blue) protein. The gray marked sequence was detected in the OxICAT screen. Cysteines in positions 83 and 84 were both replaced with serine (red). (B) Overexpression of Rab7 constructs in Neuro-2a cells. Overexpressed Rab7-WT and Rab7 redox-dead (each tagged with GFP) are distinguishable from endogenous Rab7. (C) Redox-dependent modifications affect Rab7 activity. Rab7 GTP binding (determined using an Rab7 activation assay kit) is enhanced by mutations of redox-sensitive cysteines in the Rab7 redox-dead construct (n = 3, $^*P > 0.05$). (D) Localization of Rab7 in Neuro-2a cells is not grossly affected by mutations of redox-sensitive cysteines (scale bar: 25 μm).

redox-dependent modifications of Rab7 may also arise in other tissues and cellular systems. Here, we show that a redox-insensitive mutant of Rab7 displays enhanced GTP binding, suggesting that oxidation of Rab7 terminates GTP-dependent activity of the protein. Of interest, redox-dependent processes have been recently considered as major regulators of autophagy.[14] As Rab7 is a key regulator of autophagy,[25] it remains to be elucidated whether redox-dependent modifications of Rab7 affect autophagosomal signaling in general.

We found that Rab7-knockdown mice display reduced inflammatory and ROS-induced pain behavior. In the inflammatory pain model, behavioral responses to mechanical but not thermal stimuli were significantly affected by the Rab7 knockdown, suggesting that Rab7 predominantly contributes to mechanical hypersensitivity during inflammatory pain processing. The selective role of Rab7 in zymosan-induced mechanical hyperalgesia may be explained by distinct contribution to nociceptive pathways such as TRPV1- and TRPV4-dependent pain signaling, which modulate thermal and mechanical hypersensitivity, respectively. Although TRPV1 predominantly seems to modulate thermal hyperalgesia, TRPV4 is involved in mechanical hypersensitivity after zymosan-induced hind paw inflammation.[71] Of interest, both Rab7 and TRPV4 have been associated with Charcot–Marie–Tooth disease.[17,50] Moreover, Rab7 translocated from the central terminals to the somata of sensory neurons after zymosan injection into a hind paw, further supporting our observation that Rab7 affects inflammatory pain signaling.

Previous studies point towards interactions of Rab7 with different players in pain signaling. For example, during diabetic neuropathy in rats, Rab7 co-localizes with μ-opioid receptors in perinuclear lysosome compartments, thereby promoting lysosomal targeting of μ-opioid receptors and reducing opioid responsiveness.[55] Furthermore, Rab7 controls endosomal trafficking of the nerve growth factor receptor TrkA, a key regulator of hyperalgesia.[51,53,66,77] Rab7 also interacts with calcium-/calmodulin-dependent protein kinase 4, which has been implicated in nicotine-induced pain processing.[20,28] Hence, Rab7 as a key regulator of endosomal traffic might control various pain-relevant signaling mechanisms. Altogether, these findings are consistent with the idea that redox modulations of distinct proteins such as Rab7 make an essential contribution to pain processing.

Conflicts of interest statement

The authors have no conflicts of interest to declare.

This work was supported by the Deutsche Forschungsgemeinschaft DFG-SFB 815 (A12, A14 and Z1) and the State of Hessia LOEWE-Center for Translational Medicine and Pharmacology.

Acknowledgements

The authors thank Prof Fan Wang (fan.wang@duke.edu) for providing Advillin-Cre mice. Furthermore, we thank Karin Schilling, Christine Manderscheid, Cyntia Schaefer, Ulrike Hermanni, Sylvia Oßwald, and Maximilian Mattil for excellent technical assistance.

Article history:
Received 14 September 2016
Received in revised form 21 March 2017
Accepted 3 April 2017
Available online 7 April 2017

References

[1] Basbaum AI, Bautista DM, Scherrer G, Julius D. Cellular and molecular mechanisms of pain. Cell 2009;139:267–84.

[2] Berger JV, Deumens R, Goursaud S, Schafer S, Lavand'homme P, Joosten EA, Hermans E. Enhanced neuroinflammation and pain hypersensitivity after peripheral nerve injury in rats expressing mutated superoxide dismutase 1. J Neuroinflammation 2011;8:33.
[3] Bucci C, De Luca M. Molecular basis of Charcot-Marie-Tooth type 2B disease. Biochem Soc Trans 2012;40:1368–72.
[4] Burgoyne JR, Eaton P. A rapid approach for the detection, quantification, and discovery of novel sulfenic acid or S-nitrosothiol modified proteins using a biotin-switch method. Methods Enzymol 2010;473:281–303.
[5] Cataldo AM, Mathews PM, Boiteau AB, Hassinger LC, Peterhoff CM, Jiang Y, Mullaney K, Neve RL, Gruenberg J, Nixon RA. Down syndrome fibroblast model of Alzheimer-related endosome pathology: accelerated endocytosis promotes late endocytic defects. Am J Pathol 2008;173: 370–84.
[6] Chen XQ, Wang B, Wu C, Pan J, Yuan B, Su YY, Jiang XY, Zhang X, Bao L. Endosome-mediated retrograde axonal transport of P2X3 receptor signals in primary sensory neurons. Cell Res 2012;22:677–96.
[7] Cherry S, Jin EJ, Ozel MN, Lu Z, Agi E, Wang D, Jung WH, Epstein D, Meinertzhagen IA, Chan CC, Hiesinger PR. Charcot-Marie-Tooth 2B mutations in rab7 cause dosage-dependent neurodegeneration due to partial loss of function. Elife 2013;2:e01064.
[8] Cogli L, Piro F, Bucci C. Rab7 and the CMT2B disease. Biochem Soc Trans 2009;37(pt 5):1027–31.
[9] Cohen MR, Johnson WM, Pilat JM, Kiselar J, DeFrancesco-Lisowitz A, Zigmond RE, Moiseenkova-Bell VY. Nerve growth factor regulates transient receptor potential vanilloid 2 via extracellular signal-regulated kinase signaling to enhance neurite outgrowth in developing neurons. Mol Cell Biol 2015;35:4238–52.
[10] De Luca A, Progida C, Spinosa MR, Alifano P, Bucci C. Characterization of the Rab7K157N mutant protein associated with Charcot-Marie-Tooth type 2B. Biochem Biophys Res Commun 2008;372:283–7.
[11] Deinhardt K, Salinas S, Verastegui C, Watson R, Worth D, Hanrahan S, Bucci C, Schiavo G. Rab5 and Rab7 control endocytic sorting along the axonal retrograde transport pathway. Neuron 2006;52:293–305.
[12] Dinter E, Saridaki T, Nippold M, Plum S, Diederichs L, Komnig D, Fensky L, May C, Marcus K, Voigt A, Schulz JB, Falkenburger BH. Rab7 induces clearance of alpha-synuclein aggregates. J Neurochem 2016; 138:758–74.
[13] Evans JG, Todorovic SM. Redox and trace metal regulation of ion channels in the pain pathway. Biochem J 2015;470:275–80.
[14] Filomeni G, De Zio D, Cecconi F. Oxidative stress and autophagy: the clash between damage and metabolic needs. Cell Death Differ 2015;22: 377–88.
[15] Forrester MT, Foster MW, Benhar M, Stamler JS. Detection of protein S-nitrosylation with the biotin-switch technique. Free Radic Biol Med 2009; 46:119–26.
[16] Fourquet S, Guerois R, Biard D, Toledano MB. Activation of NRF2 by nitrosative agents and H2O2 involves KEAP1 disulfide formation. J Biol Chem 2010;285:8463–71.
[17] Gentil BJ, Cooper L. Molecular basis of axonal dysfunction and traffic impairments in CMT. Brain Res Bull 2012;88:444–53.
[18] Greenspan JD, Craft RM, LeResche L, Arendt-Nielsen L, Berkley KJ, Fillingim RB, Gold MS, Holdcroft A, Lautenbacher S, Mayer EA, Mogil JS, Murphy AZ, Traub RJ; Consensus Working Group of the Sex G, Pain SIGotI. Studying sex and gender differences in pain and analgesia: a consensus report. Pain 2007;132(suppl 1):S26–45.
[19] Hacimuftuoglu A, Handy CR, Goettl VM, Lin CG, Dane S, Stephens RL Jr. Antioxidants attenuate multiple phases of formalin-induced nociceptive response in mice. Behav Brain Res 2006;173:211–16.
[20] Harrison BJ, Flight RM, Gomes C, Venkat G, Ellis SR, Sankar U, Twiss JL, Rouchka EC, Petruska JC. IB4-binding sensory neurons in the adult rat express a novel 3' UTR-extended isoform of CaMK4 that is associated with its localization to axons. J Comp Neurol 2014;522:308–36.
[21] Hasegawa H, Abbott S, Han BX, Qi Y, Wang F. Analyzing somatosensory axon projections with the sensory neuron-specific Advillin gene. J Neurosci 2007;27:14404–14.
[22] Heine S, Michalakis S, Kallenborn-Gerhardt W, Lu R, Lim HY, Weiland J, Del Turco D, Deller T, Tegeder I, Biel M, Geisslinger G, Schmidtko A. CNGA3: a target of spinal nitric oxide/cGMP signaling and modulator of inflammatory pain hypersensitivity. J Neurosci 2011;31:11184–92.
[23] Held JM, Danielson SR, Behring JB, Atsriku C, Britton DJ, Puckett RL, Schilling B, Campisi J, Benz CC, Gibson BW. Targeted quantitation of site-specific cysteine oxidation in endogenous proteins using a differential alkylation and multiple reaction monitoring mass spectrometry approach. Mol Cell Proteomics 2010;9:1400–10.
[24] Houlden H, King RH, Muddle JR, Warner TT, Reilly MM, Orrell RW, Ginsberg L. A novel RAB7 mutation associated with ulcero-mutilating neuropathy. Ann Neurol 2004;56:586–90.
[25] Hyttinen JM, Niittykoski M, Salminen A, Kaarniranta K. Maturation of autophagosomes and endosomes: a key role for Rab7. Biochim Biophys Acta 2013;1833:503–10.
[26] Ibi M, Matsuno K, Shiba D, Katsuyama M, Iwata K, Kakehi T, Nakagawa T, Sango K, Shirai Y, Yokoyama T, Kaneko S, Saito N, Yabe-Nishimura C. Reactive oxygen species derived from NOX1/NADPH oxidase enhance inflammatory pain. J Neurosci 2008;28:9486–94.
[27] Im YB, Jee MK, Jung JS, Choi JI, Jang JH, Kang SK. miR23b ameliorates neuropathic pain in spinal cord by silencing NADPH oxidase 4. Antioxid Redox Signal 2012;16:1046–60.
[28] Jackson KJ, Damaj MI. Calcium/calmodulin-dependent protein kinase IV mediates acute nicotine-induced antinociception in acute thermal pain tests. Behav Pharmacol 2013;24:689–92.
[29] Janssen-Heininger YM, Mossman BT, Heintz NH, Forman HJ, Kalyanaraman B, Finkel T, Stamler JS, Rhee SG, van der Vliet A. Redox-based regulation of signal transduction: principles, pitfalls, and promises. Free Radic Biol Med 2008;45:1–17.
[30] Ji RR, Xu ZZ, Gao YJ. Emerging targets in neuroinflammation-driven chronic pain. Nat Rev Drug Discov 2014;13:533–48.
[31] Johannes CB, Le TK, Zhou X, Johnston JA, Dworkin RH. The prevalence of chronic pain in United States adults: results of an Internet-based survey. J Pain 2010;11:1230–9.
[32] Kallenborn-Gerhardt W, Hohmann SW, Syhr KM, Schroder K, Sisignano M, Weigert A, Lorenz JE, Lu R, Brune B, Brandes RP, Geisslinger G, Schmidtko A. Nox2-dependent signaling between macrophages and sensory neurons contributes to neuropathic pain hypersensitivity. PAIN 2014;155:2161–70.
[33] Kallenborn-Gerhardt W, Lu R, Bothe A, Thomas D, Schlaudraff J, Lorenz JE, Lippold N, Real CI, Ferreiros N, Geisslinger G, Del Turco D, Schmidtko A. Phosphodiesterase 2A localized in the spinal cord contributes to inflammatory pain processing. Anesthesiology 2014;121:372–82.
[34] Kallenborn-Gerhardt W, Lu R, Syhr KM, Heidler J, von Melchner H, Geisslinger G, Bangsow T, Schmidtko A. Antioxidant activity of sestrin 2 controls neuropathic pain after peripheral nerve injury. Antioxid Redox Signal 2013;19:2013–23.
[35] Kallenborn-Gerhardt W, Schroder K, Del Turco D, Lu R, Kynast K, Kosowski J, Niederberger E, Shah AM, Brandes RP, Geisslinger G, Schmidtko A. NADPH oxidase-4 maintains neuropathic pain after peripheral nerve injury. J Neurosci 2012;32:10136–45.
[36] Kallenborn-Gerhardt W, Schroder K, Geisslinger G, Schmidtko A. NOXious signaling in pain processing. Pharmacol Ther 2013;137: 309–17.
[37] Kettenhofen NJ, Wood MJ. Formation, reactivity, and detection of protein sulfenic acids. Chem Res Toxicol 2010;23:1633–46.
[38] Kim D, You B, Jo EK, Han SK, Simon MI, Lee SJ. NADPH oxidase 2-derived reactive oxygen species in spinal cord microglia contribute to peripheral nerve injury-induced neuropathic pain. Proc Natl Acad Sci U S A 2010;107:14851–6.
[39] Ko YK, Youn AM, Hong BH, Kim YH, Shin YS, Kang PS, Yoon KJ, Lee WH. Antinociceptive effect of phenyl N-tert-butylnitrone, a free radical scavenger, on the rat formalin test. Korean J Anesthesiol 2012;62:558–64.
[40] Kozai D, Ogawa N, Mori Y. Redox regulation of transient receptor potential channels. Antioxid Redox Signal 2014;21:971–86.
[41] Kwan KY, Allchorne AJ, Vollrath MA, Christensen AP, Zhang DS, Woolf CJ, Corey DP. TRPA1 contributes to cold, mechanical, and chemical nociception but is not essential for hair-cell transduction. Neuron 2006; 50:277–89.
[42] Leichert LI, Gehrke F, Gudiseva HV, Blackwell T, Ilbert M, Walker AK, Strahler JR, Andrews PC, Jakob U. Quantifying changes in the thiol redox proteome upon oxidative stress in vivo. Proc Natl Acad Sci U S A 2008; 105:8197–202.
[43] Lim H, Kim D, Lee SJ. Toll-like receptor 2 mediates peripheral nerve injury-induced NADPH oxidase 2 expression in spinal cord microglia. J Biol Chem 2013;288:7572–9.
[44] Lipton SA, Choi YB, Takahashi H, Zhang D, Li W, Godzik A, Bankston LA. Cysteine regulation of protein function–as exemplified by NMDA-receptor modulation. Trends Neurosci 2002;25:474–80.
[45] Lorenz JE, Kallenborn-Gerhardt W, Lu R, Syhr KM, Eaton P, Geisslinger G, Schmidtko A. Oxidant-induced activation of cGMP-dependent protein kinase Ialpha mediates neuropathic pain after peripheral nerve injury. Antioxid Redox Signal 2014;21:1504–15.
[46] Lu R, Bausch AE, Kallenborn-Gerhardt W, Stoetzer C, Debruin N, Ruth P, Geisslinger G, Leffler A, Lukowski R, Schmidtko A. Slack channels expressed in sensory neurons control neuropathic pain in mice. J Neurosci 2015;35:1125–35.
[47] Lu R, Kallenborn-Gerhardt W, Geisslinger G, Schmidtko A. Additive antinociceptive effects of a combination of vitamin C and vitamin E after peripheral nerve injury. PLoS One 2011;6:e29240.

[48] Lu R, Lukowski R, Sausbier M, Zhang DD, Sisignano M, Schuh CD, Kuner R, Ruth P, Geisslinger G, Schmidtko A. BKCa channels expressed in sensory neurons modulate inflammatory pain in mice. PAIN 2014;155: 556–65.
[49] Macovei A, Petrareanu C, Lazar C, Florian P, Branza-Nichita N. Regulation of hepatitis B virus infection by Rab5, Rab7, and the endolysosomal compartment. J Virol 2013;87:6415–27.
[50] Manganelli F, Nolano M, Pisciotta C, Provitera V, Fabrizi GM, Cavallaro T, Stancanelli A, Caporaso G, Shy ME, Santoro L. Charcot-Marie-Tooth disease: new insights from skin biopsy. Neurology 2015;85:1202–8.
[51] McKelvey L, Shorten GD, O'Keeffe GW. Nerve growth factor-mediated regulation of pain signalling and proposed new intervention strategies in clinical pain management. J Neurochem 2013;124:276–89.
[52] Meller ST, Gebhart GF. Intraplantar zymosan as a reliable, quantifiable model of thermal and mechanical hyperalgesia in the rat. Eur J Pain 1997; 1:43–52.
[53] Mizumura K, Murase S. Role of nerve growth factor in pain. Handb Exp Pharmacol 2015;227:57–77.
[54] Mogil JS, Chanda ML. The case for the inclusion of female subjects in basic science studies of pain. PAIN 2005;117:1–5.
[55] Mousa SA, Shaqura M, Khalefa BI, Zollner C, Schaad L, Schneider J, Shippenberg TS, Richter JF, Hellweg R, Shakibaei M, Schafer M. Rab7 silencing prevents mu-opioid receptor lysosomal targeting and rescues opioid responsiveness to strengthen diabetic neuropathic pain therapy. Diabetes 2013;62:1308–19.
[56] Niemann A, Berger P, Suter U. Pathomechanisms of mutant proteins in Charcot-Marie-Tooth disease. Neuromolecular Med 2006;8:217–42.
[57] Olsen JV, de Godoy LM, Li G, Macek B, Mortensen P, Pesch R, Makarov A, Lange O, Horning S, Mann M. Parts per million mass accuracy on an Orbitrap mass spectrometer via lock mass injection into a C-trap. Mol Cell Proteomics 2005;4:2010–21.
[58] Osteen JD, Herzig V, Gilchrist J, Emrick JJ, Zhang C, Wang X, Castro J, Garcia-Caraballo S, Grundy L, Rychkov GY, Weyer AD, Dekan Z, Undheim EA, Alewood P, Stucky CL, Brierley SM, Basbaum AI, Bosmans F, King GF, Julius D. Selective spider toxins reveal a role for the Nav1.1 channel in mechanical pain. Nature 2016;534:494–9.
[59] Ponomareva OY, Eliceiri KW, Halloran MC. Charcot-Marie-Tooth 2b associated Rab7 mutations cause axon growth and guidance defects during vertebrate sensory neuron development. Neural Dev 2016;11:2.
[60] Raisanen SR, Halleen J, Parikka V, Vaananen HK. Tartrate-resistant acid phosphatase facilitates hydroxyl radical formation and colocalizes with phagocytosed Staphylococcus aureus in alveolar macrophages. Biochem Biophys Res Commun 2001;288:142–50.
[61] Rak A, Pylypenko O, Niculae A, Pyatkov K, Goody RS, Alexandrov K. Structure of the Rab7:REP-1 complex: insights into the mechanism of Rab prenylation and choroideremia disease. Cell 2004;117:749–60.
[62] Riffel AP, de Souza JA, Santos MD, Horst A, Scheid T, Kolberg C, Bello-Klein A, Partata WA. Systemic administration of vitamins C and E attenuates nociception induced by chronic constriction injury of the sciatic nerve in rats. Brain Res Bull 2016;121:167–77.
[63] Roy SG, Stevens MW, So L, Edinger AL. Reciprocal effects of rab7 deletion in activated and neglected T cells. Autophagy 2013;9:1009–23.
[64] Rudyk O, Eaton P. Biochemical methods for monitoring protein thiol redox states in biological systems. Redox Biol 2014;2:803–13.
[65] Salvemini D, Little JW, Doyle T, Neumann WL. Roles of reactive oxygen and nitrogen species in pain. Free Radic Biol Med 2011;51:951–66.
[66] Saxena S, Bucci C, Weis J, Kruttgen A. The small GTPase Rab7 controls the endosomal trafficking and neuritogenic signaling of the nerve growth factor receptor TrkA. J Neurosci 2005;25:10930–40.
[67] Schmidtko A, Gao W, Konig P, Heine S, Motterlini R, Ruth P, Schlossmann J, Koesling D, Niederberger E, Tegeder I, Friebe A, Geisslinger G. cGMP produced by NO-sensitive guanylyl cyclase essentially contributes to inflammatory and neuropathic pain by using targets different from cGMP-dependent protein kinase I. J Neurosci 2008;28:8568–76.
[68] Schnell SA, Staines WA, Wessendorf MW. Reduction of lipofuscin-like autofluorescence in fluorescently labeled tissue. J Histochem Cytochem 1999;47:719–30.
[69] Schwartz ES, Kim HY, Wang J, Lee I, Klann E, Chung JM, Chung K. Persistent pain is dependent on spinal mitochondrial antioxidant levels. J Neurosci 2009;29:159–68.
[70] Schwartz ES, Lee I, Chung K, Chung JM. Oxidative stress in the spinal cord is an important contributor in capsaicin-induced mechanical secondary hyperalgesia in mice. PAIN 2008;138:514–24.
[71] Segond von Banchet G, Boettger MK, Konig C, Iwakura Y, Brauer R, Schaible HG. Neuronal IL-17 receptor upregulates TRPV4 but not TRPV1 receptors in DRG neurons and mediates mechanical but not thermal hyperalgesia. Mol Cell Neurosci 2013;52:152–60.
[72] Solorzano C, Villafuerte D, Meda K, Cevikbas F, Braz J, Sharif-Naeini R, Juarez-Salinas D, Llewellyn-Smith IJ, Guan Z, Basbaum AI. Primary afferent and spinal cord expression of gastrin-releasing peptide: message, protein, and antibody concerns. J Neurosci 2015;35: 648–57.
[73] Spinosa MR, Progida C, De Luca A, Colucci AM, Alifano P, Bucci C. Functional characterization of Rab7 mutant proteins associated with Charcot-Marie-Tooth type 2B disease. J Neurosci 2008;28:1640–8.
[74] Verhoeven K, De Jonghe P, Coen K, Verpoorten N, Auer-Grumbach M, Kwon JM, FitzPatrick D, Schmedding E, De Vriendt E, Jacobs A, Van Gerwen V, Wagner K, Hartung HP, Timmerman V. Mutations in the small GTP-ase late endosomal protein RAB7 cause Charcot-Marie-Tooth type 2B neuropathy. Am J Hum Genet 2003;72:722–7.
[75] Wang T, Ming Z, Xiaochun W, Hong W. Rab7: role of its protein interaction cascades in endo-lysosomal traffic. Cell Signal 2011;23:516–21.
[76] Zhang M, Chen L, Wang S, Wang T. Rab7: roles in membrane trafficking and disease. Biosci Rep 2009;29:193–209.
[77] Zhang K, Fishel Ben Kenan R, Osakada Y, Xu W, Sinit RS, Chen L, Zhao X, Chen JY, Cui B, Wu C. Defective axonal transport of Rab7 GTPase results in dysregulated trophic signaling. J Neurosci 2013;33:7451–62.
[78] Zhang Y, Keszler A, Broniowska KA, Hogg N. Characterization and application of the biotin-switch assay for the identification of S-nitrosated proteins. Free Radic Biol Med 2005;38:874–81.
[79] Zurborg S, Piszczek A, Martinez C, Hublitz P, Al Banchaabouchi M, Moreira P, Perlas E, Heppenstall PA. Generation and characterization of an Advillin-Cre driver mouse line. Mol Pain 2011;7:66.